Booster Adhesion of Crystalline Poly(vinylidene fluoride) Binder by Heat Treatment for Ni-rich Layered Oxide Cathode in Lithium-ion Batteries

Jineun Kim,[a] Suhyun Lee,[a] Seonghun Jeong,[b] Meihua Hong,[b] Van-Chuong Ho,[b] Yeong Don Park,[a] Ki Jae Kim,*[c, d] and Junyoung Mun*[a, b, d]

Abstract: High energy density of lithium-ion batteries is crucial for highly efficient battery systems. Ni-rich layered oxide cathode materials with a high specific capacity have garnered considerable interest. Ni-rich cathode materials exhibit rather large volume fluctuations during charging and discharging, unlike traditional cathode materials. This study investigated the electrochemical performance of a Ni-rich cathode with a focus on controlling binder adhesion of poly(vinylidene fluoride) (PVDF), which is the most feasible cathode binder for battery manufacturing, to mitigate the failure mode of volume changes. A simple heat treatment of 200 °C over melting point is effective to enhance binding force by altering nanoscale alignment of PVDF. The study evaluates the electrochemical properties of the Ni-rich cathode with different levels of binder adhesion to determine the optimal binder conditions for high performance.

1. Introduction

Climate change is a critical issue casued by burning fossil fuels, leading to the need for sustainable systems.[1,2] Lithium-ion batteries (LIBs) play a key role by storing and using renewable energy, which has fluctuating resources. The growing demand for larger LIBs in energy stroage systems (ESS), and electric vehicles (EV) requires ongoing research to improve their performance, especially high energy density. For use in renewable energy storage systems and electric vehicles has led to a need for higher energy density batteries. Additionally, the cost of these batteries has also increased due to their size and complexity, making it important to find ways to make them more affordable and sustainable.

[a] J. Kim, S. Lee, Prof. Y. D. Park, Prof. J. Mun
Department of Energy and Chemical Engineering
Incheon National University
119 Academy-ro, Yeonsu-gu, Incheon, 22012 (Republic of Korea)

[b] S. Jeong, M. Hong, Dr. V.-C. Ho, Prof. J. Mun
School of Advanced Materials Science & Engineering
Sungkyunkwan University
2066, Seobu-ro, Jangan-gu, Suwon-si, Gyeonggi-do 16419 (Republic of Korea)
E-mail: munjy@skku.edu

[c] Prof. K. Kim
Department of Energy Science
Sungkyunkwan University
2066, Seobu-ro, Jangan-gu, Suwon-si, Gyeonggi-do 16419 (Republic of Korea)
E-mail: kijaekim@skku.edu

[d] Prof. K. Kim, Prof. J. Mun
SKKU Institute of Energy Science and Technology (SIEST)
Sungkyunkwan University
2066, Seobu-ro, Jangan-gu, Suwon-si, Gyeonggi-do 16419 (Republic of Korea)

Ni-rich layered oxide cathode is one of the top candidate for high energy density LIBs. Replacing Co with Ni in LiCoO$_2$ results in a higher energy density and lower cost.[3–5] The use of metal ions other than Co, such as Ni, Mn, and Al, is being actively pursued to further increase the energy density and stability of the batteries. Esepcially, the recent commerialization of Ni-rich materials as cathode active materials for LIBs is a significant step towards improving the energy density and competitiveness of LIBs.[6–8]

For manufacuring engineering, the battery and electrode fabrication technique also enhances the energy density.[9–12] It has been focused to advance manufacturing technologies, where the goal is to increase energy density by maximizing the amount of active material and minimizing the conductive material and binder. In battery electrode manufacturing process, a slurry type mixture is cast onto the current collector foil, and the electrode matrix held together by an adhesive binder. Polymers such as PVDF, styrene butadiene rubber (SBR), and polytetrafluoroethylene (PTFE), are commonly used as binders in battery electrodes.[11,13–17] An electrochemically and oxidatively stable polymer is required for the positive electrode. Additionally, the Li ions of of the cathode active materials can be dissolved in the aqueous binder solutions.[18,19] Thus, the use of PVDF and NMP solvent is a representative system for LIB-cathode manufacturing.

Research continues to focus on improving the performance of LIBs by developing better binders. Currently, most research for battery binder has been focused on high capacity anodes with severe volume changes and binders such as polyacrylic acid (PAA) and polyimide (PI) are being developed for Si and Sn anodes.[20–22] Relatively, cathode materials have been known as more stable matrix with relatively small volume change. Thus, there is limited research on the use of binders to enhance the physical characteristics for cathode materials.

Ni-rich cathode materials with high energy density are known to exhibit comparatively high lattice parameter changes

during cycling by the recent papers.[23,24] It is known that this characteristics cause microcracks of secondary particles during the charging and discharging process of Ni-rich materials, which are predominantly produced through a co-precipitation synthetic method.[25–28] It increases the resistance by restricting the electron transfer path in the electrode. Several recent researches have reported on the improvement of binder binding force for high performance of Ni-rich layered oxide materials. by controlling the interface of cathode materials or by employing strong spandex-based binder materials. Choi reported a strong binder of spandex to hold Ni-rich cathode particles tightly during cycling. Also, Jeong reported a surface modification of Ni-rich layered oxide by perfluorinated molecular functional coating to enhance adhesive force between PVDF binder and active material surface.[3,29]

In this study, the aim is to improve the binding force of the PVDF binder commonly used in conventional battery production. A very small amount, 2 wt.%, of PVDF was used to response the manufacturing process for high energy density of LIBs. Polymers with high crystallinity are generally stiffer, have greater tensile strength, and exhibit higher recoverable strain, resulting in increased strength and durability. It is known that the crystalline polymers exhibit high adhesive force than amorphous polymers by changing their nano scale interaction.[30–32] Heat treatment is a simple process to introduce crystallinity onto polymers. Heat-treated PVDF was chosen due to its low melting point and the ability to enhance crystallinity within the temperature range accessible in the electrode production process. The focus was on Ni-rich materials, as the binder was found to play an important role in their performance, and research was conducted to ensure the long-lasting features of Ni-rich electrodes.

2. Results and Discussion

The thermal analysis was conducted using DSC and TGA techniques (Figure 1a, and Figure S1). The goal of the thermal analysis was to evaluate the thermal properties of the PVDF binder, such as its melting point, thermal stability, and degradation behavior. In the DSC curve shown in Figure 1a, an endothermic peak at approximately 174°C corresponds to the reorited PVDF melting point.[33] In addition, a reversible exothermic peak at 134°C on the cooling curve proved to be freezing and it also confirms the endotherthermic peak was originated from melting.[33,34] In Figure S1, the TGA analysis of PVDF showed a weight loss of 4 wt.% below 100°C, due to the elimination of internal moisture. Above 100°C, a stable TGA curve was observed up to 430°C. The results of the thermal analysis provide insights into the thermal properties of the PVDF binder, including its melting point and thermal stability as well. By a binder electrode coated only with PVDF, heat treatment was carried out at various temperatures, and crystallinity was determined using XRD analyses. The associated results are depicted in Figure 1b. First, the XRD investigation of the binder electrode with 120°C heat treatment revealed no unique peak. This indicates that the PVDF coating's crystallinity
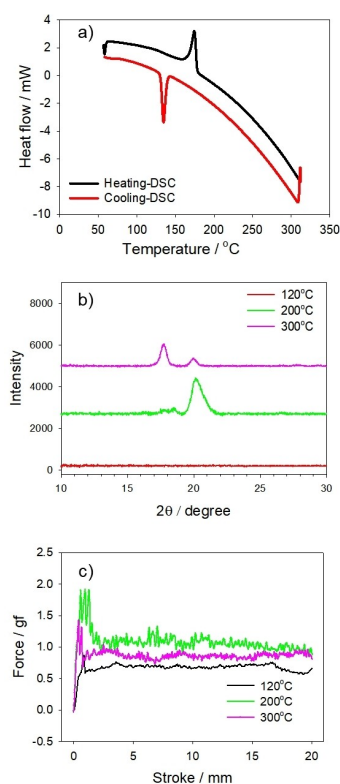

Figure 1. a) DSC analyses of the PVDF binder powder. b) XRD patterns and c) adhesive force of the binder electrode without active material and conducting agent after additional heat treatment of 120, 200 and 300°C

is close to amorphous statues. However, the sample treated at 200°C (red line) displays a beta PVDF-identifiable crystalline diffraction peak near 20°.[35] It was confirmed that crystallinity increased as the temperature of the heat treatment rose. At high temperatures, such as 300 degrees, the XRD peak corresponding to the alpha phase near 18° was noticed more prominently. The binding strength of binders treated at higher temperatures, such as 200 and 300°C for the heat treatment of the binder electrode, was greater than that of binders treated using the 120°C procedure. Usually, 120°C drying condition is applying for electrode fabrication procedure to eliminate NMP solvent. The results of a UTM evaluation of the binding force are reported in Figure 1c. This is typically associated with the increase in crystallinity resulting from the increase in fluidity of the chain following heat treatment at a temperature above the melting point of the binder. In general, the resulting crystalline binder exhibits greater adherence. However, heat treatment at 300°C is anticipated to yield alpha PVDF with relatively low electrostatic attraction.

A fundamental electrochemical evaluation was conducted using a 2032 half cell with Ni-rich layered oxide composite electrode. First, the crystallinity of the cathode active material was unaffected by heat treatment (Figure S2). Even after the heat treatment, the XRD pattern of the composite electrode had a well-known layered structural pattern and exhibited the same crystallinity of the pristine electrode. This indicates that the experimental heat treatment technique had no effect on

the layered cathode crystalline structure. This is because the positive electrode material and the binder are thermally stable at heat-treatment temperature. The electrochemical evaluation showed that the Ni-rich layered oxide cathode material had a declining specific capacity with increasing current density. The higher the current, the worse the cycleability. As shown in Figure S3a, the specific capacity declined to 137.9, and 67.5 mAh g^{-1} after 100 cycles at 0.3, and 1 C charge/discharge current densities, respectively. Specifically, in red dots for 1 C cycling, when the current was reduced from 1 to 0.1 C after the 120th cycle, the capacity increased from 33.0 to 92.8 mAh g^{-1}. This indicates that a large amount of the capacity loss of the cathode electrode was caused by the increase in kinetic resistance. For this, the relief of kinetic resistance by lowering current density contributed the capacity increasement.

In comparison to the composite electrode without additional heat treatment (described as pristine), the electrochemical performance of the composite electrode with heat treated binder was enhanced. The cycleability features of the three Ni-rich composite electrodes with different heat treatment conditions are depicted in Figure 2a. At the 100th cycle, the capacity of the composite electrode without any specific heat treatment was measured to be 97.6 mAh g^{-1}. In contrast, the specific capacities of electrode samples heated at 200 and 300 °C, which are denoted as 200 HT and 300 HT, were determined to be 151.6 and 125.4 mAh g^{-1} at the same cycle number, respectively. When the capacity retention rate is represented relative to the starting capacity, a greater value is attained. The capacity retention rates of the pristine, 200 HT and 300 HT samples are determined to be 50.7, 83.7, and 69.6%, respectively. The composite electrode heated at 200 °C, which is deemed preferable to the electrode in Figure 1 with a strong binding force of the binder. In the detailed voltage profile, the first charging voltage curve resembles the curve of a typical Ni-rich sample. A voltage plateau was observed at 3.7 V vs. Li/Li$^+$

and a additional characteristic plateau was also observed at 4.2 V vs. Li/Li$^+$. On the discharge curve, reversible voltage plateaus were observed again. In the instance of the composite electrodes that were subjected to heat treatment, the initial discharge capacity was slightly low. The resistance is considered to have grown as the surface binder was dispersed during heat treatment process. This binder can hinder ionic transportation during the 1st cycle. In the subsequent cycle, the voltage curve in the pristine electrode got increasingly sluggish, and the resistance increased. However, the sample treated at 200 °C exhibited such remarkable electrode stability that the capacity was determined to be 151.6 mAh g^{-1} even after 100 cycles. The 300 HT sample likewise demonstrated great electrode safety when compared to the sample without heat treatment; however, the detailed voltage curve indicated that the 200 HT sample had a lower resistance (Figure S3b). Before cycling, the initial resistive behavior of the prepared cells were analyzed by AC impedance. The diameter of semi-cirlce in Nyquist plot (Figure S3c) also supports that the initial resistance of 300 HT sample was higher than that of 200 HT sample. It is belived that the high temperature of 300 °C caused more rigid and resistive binder characteristics by enhancing crystallinity of PVDF and surface modifications. Thus, the binder nano structure should be carefully optimized. On the other hand, the heat-treated active material powder was prepared without a binder, and subsequently, the electrode was fabricated using the same PVDF binder. When the electrode was not subjected to heat treatment, the cycleability of the electrode containing heat-treated Ni-rich active material was found to be similar with the pristine electrode with Ni-rich active material without heat-treatment (Figure S3d). It confirmed that the heat-treatment on the active material did not significantly impact its cycle life.

Through cross-sectional SEM, the greater stability of the 200 HT sample was observed. Prior to cycling, the cross-sectional SEM images of both electrodes (the pristine and 200 HT sample) were found to be similar to each other. It represents that the initial conditions of the electrodes were almost same (Figure S4). After 100 cycles, a cross-sectional sample of the electrode was obtained by a cross-sectional polisher. After the charging protocol, a gap was noticed between the current collector and electrode particles in the case of pristine (Figure 3a). It was determined that the gap was slightly reduced in the electrode resulting from discharge, although a void was present within the electrode (Figure 3b). The Ni-rich material undergoes a significant volume change while charging, and volume shrinkage occurs after 4.0 V vs. Li/Li$^+$, indicating a significant volume change.[3,27,36,37] During the discharging, the volume is secured as lithium re-enters, and the deterioration of the electrode binding force is mitigated. However, the physcial stress by charge process still remain after the discharging process. It was noticed that both the overall behavior of deterioration and the amount of vacant space in the charged electrode were greatly reduced by heat treatment (Figure 3c). The discharged 200 HT sample exhibited highly preserved electrode statues as well (Figure 3d). The top SEM images showin in Figure S5 also exhibited the strong binding characteristics of HT electrode. After charging, it was observed that there was a gap between the active material of the pristine electrode and the
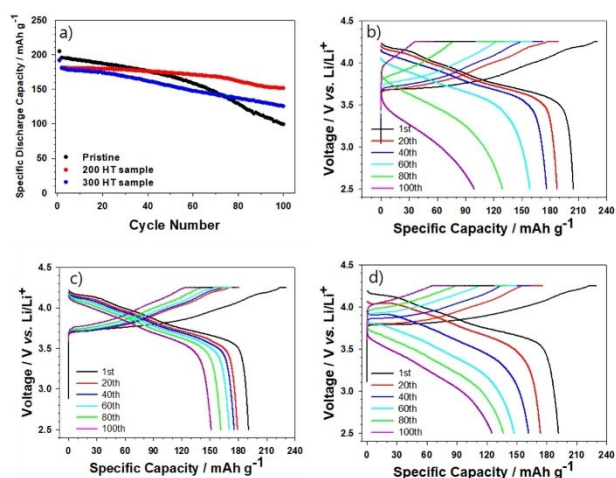

Figure 2. a) Cycleability of the Ni-rich composite electrode in 2032 coin type half cells. (Current condition: 0.2 C for the 1st cycle, and 0.5 C for the subsequent cycles, potential range of 4.3 to 2.5 V vs. Li/Li$^+$). Detail voltage profiles of the cells with b) pristine electrode, c) 200 HT electrode and d) 300 HT electrode.
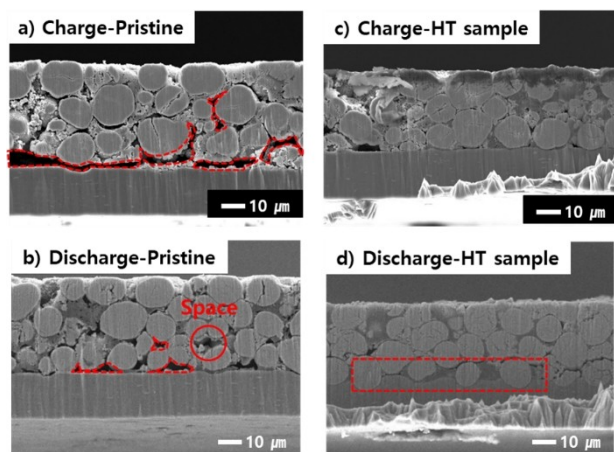
Figure 3. Cross-sectional SEM images of the pristine electrode and the 200 HT electrode after 100 cycle. a) The charged, and b) discharged pristine electrode. c) The charged, and d) discharged 200 HT electrode.

conducting agent (Figure S5a and b). However, in the 200 HT sample, such gap was observed as much as the pristine electrode (Figure S5c and d). This indicates that the binder with a high binding force by crystalline PVDF preserved the electrode stability of a Ni-rich layered oxide electrode subjected to a significant volume changes very well.

EIS was used to investigate the resistance behavior according to the cycle. After each number of cycles, the EIS in the state of charge was monitored and shown using a Nyquist plot. (Figure 4) Each plot is comprised of two semicircles, and the corresponding equivalent circuit is shown as an inset. Each diameter of semi-circle represents resistance from the surface film (R_{SEI}) for the high-frequency domain and charge transfer (R_{ct}) for the low-frequency domain. Additionally, the X-axis intercept represents the ohmic resistance. To facilitate comprehension of the frequency-dependent behavior of the two semicircles, the cyan point corresponding to 251.19 Hz is highlighted. It was determined that both samples resistance grew as each cycle progressed. As the cycle progressed, the X-axis intercept value of the heat-treated sample showed a slight increase. This indicates that the electron transfer channel was constrained as a result of the Ni-rich sample recurrent desorption due to the insufficient binding force of the previously examined binder. In addition, this indicates that the binder
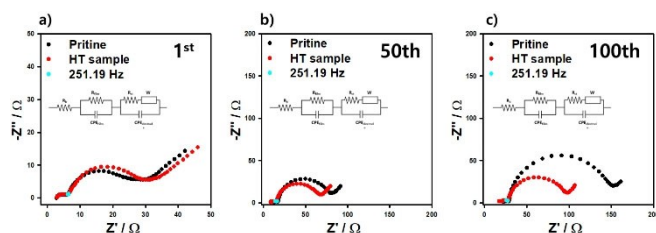
strengthened by heat treatment contributed to the stable maintenance of the Ni-rich material durability by enhancing electrode safety.

Figure S6 depicts the cycleablity of the electrode produced by the same heat treatment using $LiCoO_2$ with relatively small volume change from Ni-rich layerd oxide. In contrast to Ni-rich layered oxide materials, no substantial increase in cycle life was measured before and after heat treatment for $LiCoO_2$ composite electrode. This indicates that, unlike Ni-rich materials, the $LiCoO_2$ material does not undergo a considerable volume change, hence the gain in durability brought about by the binder is negligible. Therefore, it was established that the Ni-rich material suffers a significant volume change during the charging and discharging process, necessitating a method for enhancing the binder binding force.

3. Conclusion

In the study, the Ni-rich cathode material was found to require a strong binder due to its significant volume change during charging and discharging, which can separate the current collector from the particles in the electrode. PVDF binder, widely used in the commercial process, was employed and its binder binding force was increased by heat treatment at 200 °C to improve crystallinity, showing that high lifetime characteristics can be achieved while preserving the electrode crystal structure. The results suggest that the role of binder in the electrode of Ni-rich materials is critical and further research on binders is needed to improve the performance and longevity of high-energy density batteries using Ni-rich cathode materials.

Experimental Section

Electrochemical assessment

To prepare Ni-rich layered oxide, $Ni_{0.88}Co_{0.06}Mn_{0.06}(OH)_2$ is prepared by co-precipitation using $NiSO_4 \cdot 6H_2O$, $CoSO_4 \cdot 7H_2O$, and $MnSO_4 \cdot H_2O$. The $Ni_{0.88}Co_{0.06}Mn_{0.06}(OH)_2$ is then homogenized with lithium hydroxide in a 1:1.05 M ratio. The mixture is then calcined in an oxygen atmosphere at 750 °C for 12 hours. The prepared Ni-rich layered oxide material, super-P, and PVDF (Kureha, KF1100) were combined in a weight ratio of 96:2:2, and NMP was added to achieve a solids-to-liquids weight ratio of 60%. The electrode thickness and loading level were both carefully controlled during the experiment to be around 60 μm and 2 mAh cm^{-2}, respectively. The prepared slurry was thoroughly blended with a PDM-300 (KM tech). Using a doctor blade and a bar coater, a uniform layer of slurry was casted to the Al current collector. And NMP was thoroughly dried in a convection oven at 120 °C for approximately 10 minutes. Each electrode was subjected to a 12-hour heat treatment at a specific target temperature (120, 200, or 300 °C) in an Argon environment. The electrode was pressed through a roll pressor and punched to a diameter of 1.2 cm. After the heat treatment, the round electrode was re-dried in a vacuum atmosphere and then transported to a glove box. Using the composite electrode produced, a separator, a lithium metal disc, and 1 M LiPF$_6$/EC:DEC (Panaxetec) electrolyte, a 2032 coin cell was fabricated. After a 12-hour rest period, the 2032 coin half cells were charged to 4.25 V at a 0.2 C rate (1 C = 200 mAg^{-1}), and the cell potential was maintained at 4.25 V until the current reached 0.05 C. The discharge was then performed to 2.5 V at 0.2 C. In the second charge/discharge cycle, the charge current density

Figure 4. Nyquist plots from the charged cells (black dots: the pristine electrode, and red dots: 200 HT electrode) after the a) 1st, b) 50th, and c) 100th cycle. The equivalent circuit for spectra is shown as insets. The point measured under 251.19 Hz is highlighted by cyan color.

was increased to 0.5 C, but the subsequent charge to 4.5 V constant voltage current situation remained the same as the initial cycle condition at 0.05 C. The discharging sequence was also increased to 0.5 C and performed up to 2.5 V. This second charge/discharge condition was repeatedly conducted to carry out a cycle test. After a predetermined number of cycles, AC impedance was measured after 30 minutes of rest using the Zive Lab MP2 (Won-A-Tech).

Material evaluation

Using binder powder, differential scanning calorimeter (DSC) measurements were conducted at a maximum temperature of 300 degrees and a minimum temperature of 50 °C in a N_2 environment at a rate of 10 °C min^{-1} (Q1000, TA instrument). In addition, thermal gravimetric analyses (TGA) were conducted at 5 °C min^{-1} in an Ar environment. A PVDF NMP solution was utilized to coat an aluminum current collector. Afterwards, a binder electrode devoid of an active substance was prepared by drying at a certain temperature. The obtained electrode's binder binding force was measured using a multi-test equipment. Moreover, the produced binder electrode was measured using an XRD instrument. Prior to charging, the crystallinity of the electrode utilized for electrochemical evaluation was also assessed using XRD analysis. In order to evaluate adhesive force of binder electrode, 3 M tape was attached on the binder electrode, and the peeling force was counted by pulling off the tape by a universal testing machine (UTM, Instron 5569) After a certain charge/discharge cycle, an electrode was extracted from the coin cell. Using a cross-sectional polisher device, a cross section of the acquired electrode was created. FE-SEM examination of the obtained specimen.

Acknowledgements

Conflict of Interests

The authors declare no conflict of interest.

Data Availability Statement

The data that support the findings of this study are available on request from the corresponding author. The data are not publicly available due to privacy or ethical restrictions.

[1] M. Gutsch, J. Leker, *J. Energy Storage.* **2022**, *52*, 105030.
[2] M. Raugei, E. Leccisi, V. M. Fthenakis, *Energy Technol.* **2020**, *8*, 1901146.
[3] S. Jeong, S. Young Park, B. So, K. Tae Lee, Y. Don Park, J. Mun, *Chem. Eng. J.* **2022**, *448*, 137654.
[4] V.-C. Ho, S. Jeong, T. Yim, J. Mun, *J. Power Sources.* **2020**, *450*, 227625.
[5] J.-M. Kim, Y. Xu, M. H. Engelhard, J. Hu, H.-S. Lim, H. Jia, Z. Yang, B. E. Matthews, S. Tripathi, X. Zhang, L. Zhong, F. Lin, C. Wang, W. Xu, *ACS Appl. Mater. Interfaces.* **2022**, *14*, 17405–17414.
[6] B.-J. Chae, H. J. Song, J. Mun, T. Yim, *J. Electrochem. Sci. Technol.* **2020**, *11*, 361–367.
[7] J. Zhang, Z. Yang, R. Gao, L. Gu, Z. Hu, X. Liu, *ACS Appl. Mater. Interfaces.* **2017**, *9*, 29794–29803.
[8] P. Zhou, H. Meng, Z. Zhang, C. Chen, Y. Lu, J. Cao, F. Cheng, J. Chen, *J. Mater. Chem. A.* **2017**, *5*, 2724–2731.
[9] A. Laforgue, X. Z. Yuan, A. Platt, S. Brueckner, F. Perrin-Sarazin, M. Toupin, J. Y. Huot, A. Mokrini, *J. Power Sources.* **2022**, *524*, 231071.
[10] S. Niu, S. Heng, G. Zhu, J. Xu, Q. Qu, K. Wu, H. Zheng, *J. Energy Storage.* **2021**, *44*, 103425.
[11] G. Park, J.-S. Park, H.-S. Kim, K. J. Lee, *Carbon Lett.* **2022**, *32*, 265–272.
[12] K. Borzutzki, M. Winter, G. Brunklaus, *J. Electrochem. Soc.* **2020**, *167*, 070546.
[13] K. K. Rajeev, E. Kim, J. Nam, S. Lee, J. Mun, T.-H. Kim, *Electrochim. Acta.* **2020**, *333*, 135532.
[14] S. Hu, L. Wang, T. Huang, A. Yu, *J. Power Sources.* **2020**, *449*, 227472.
[15] S. Lee, J. Jang, D. Lee, J. Kim, J. Mun, *Int. J. Energy Res.* **2022**, *46*, 6480–6486.
[16] Q. D. Nguyen, K. H. Chung, *Appl. Phys. Lett.* **2020**, *116*, 061604.
[17] X. Yan, Y. Zhang, K. Zhu, Y. Gao, D. Zhang, G. Chen, C. Wang, Y. Wei, *J. Power Sources.* **2014**, *246*, 95–102.
[18] H. Chen, M. Ling, L. Hencz, H. Y. Ling, G. Li, Z. Lin, G. Liu, S. Zhang, *Chem. Rev.* **2018**, *118*, 8936–8982.
[19] I. Bloom, J. Bareño, N. Dietz Rago, F. Dogan, D. G. Graczyk, Y. Tsai, S. R. Naik, S. D. Han, E. Lee, Z. Du, Y. Sheng, J. Li, D. L. Wood, III, L. A. Steele, J. Lamb, S. Spangler, C. Grosso, K. Fenton, *J. Power Sources.* **2018**, *385*, 156–164.
[20] M. Hong, S. Lee, S. Choi, J. Mun, *J. Electroanal. Chem.* **2020**, *871*, 114317.
[21] S. Y. Lee, Y. Choi, K. S. Hong, J. K. Lee, J. Y. Kim, J. S. Bae, E. D. Jeong, *Appl. Surf. Sci.* **2018**, *447*, 442–451.
[22] C. Li, C. Liu, K. Ahmed, Z. Mutlu, Y. Yan, I. Lee, M. Ozkan, C. S. Ozkan, *RSC Adv.* **2017**, *7*, 36541–36549.
[23] G. W. Nam, N.-Y. Park, K.-J. Park, J. Yang, J. Liu, C. S. Yoon, Y.-K. Sun, *ACS Energy Lett.* **2019**, *4*, 2995–3001.
[24] Y. Su, Q. Zhang, L. Chen, L. Bao, Y. Lu, S. Chen, F. Wu, *J. Energy Chem.* **2022**, *65*, 236–253.
[25] F. Schipper, E. M. Erickson, C. Erk, J. Y. Shin, F. F. Chesneau, D. Aurbach, *J. Electrochem. Soc.* **2017**, *164*, A6220–A6228.
[26] X. Liu, B. Zheng, J. Zhao, W. Zhao, Z. Liang, Y. Su, C. Xie, K. Zhou, Y. Xiang, J. Zhu, H. Wang, G. Zhong, Z. Gong, J. Huang, Y. Yang, *Adv. Energy Mater.* **2021**, *11*, 2003583.
[27] S. Jeong, J. H. Park, S. Y. Park, J. Kim, K. T. Lee, Y. D. Park, J. Mun, *ACS Appl. Mater. Interfaces.* **2021**, *13*, 22475–22484.
[28] U.-H. Kim, G.-T. Park, B.-K. Son, G. W. Nam, J. Liu, L.-Y. Kuo, P. Kaghazchi, C. S. Yoon, Y.-K. Sun, *Nat. Energy.* **2020**, *5*, 860–869.
[29] B. Chang, J. Kim, Y. Cho, I. Hwang, M. S. Jung, K. Char, K. T. Lee, K. J. Kim, J. W. Choi, *Adv. Energy Mater.* **2020**, *10*, 2001069.
[30] S. Arabnejad, K. Yamashita, S. Manzhos, *Phys. Chem. Chem. Phys.* **2017**, *19*, 7560–7567.
[31] W. Wang, G. Zhao, X. Wu, Z. Zhai, *J. Appl. Polym. Sci.* **2015**, *132*, 42773.
[32] M. Danek, M. Lutomski, W. Maniukiewicz, M. Kozanecki, *Polym. Adv. Technol.* **2021**, *32*, 1272–1287.
[33] E. Erdtman, K. C. Satyanarayana, K. Bolton, *Polymer.* **2012**, *53*, 2919–2926.
[34] P. Saxena, P. Shukla, *Adv. Compos. Hybrid. Mater.* **2021**, *4*, 8–26.
[35] J. W. Han, B. K. Park, S. Y. Yang, J. Lee, J. Mun, J. W. Choi, K. J. Kim, *ACS Appl. Mater. Interfaces.* **2022**, *14*, 48570–48581.
[36] W. Zhao, J. Zheng, L. Zou, H. Jia, B. Liu, H. Wang, M. H. Engelhard, C. Wang, W. Xu, Y. Yang, J. G. Zhang, *Adv. Energy Mater.* **2018**, *8*, 1800297.
[37] S. Jeong, K. Choi, V.-C. Ho, J. Cho, J.-S. Bae, S. C. Nam, T. Yim, J. Mun, *Chem. Eng. J.* **2022**, *434*, 134577.